arXiv:cond-mat/0606737v2 [cond-mat.dis-nn] 29 Jun 2006

The study of electronic and magnetic properties of the partially disordered pseudo-Heusler alloy $Co_2Fe_{0.4}Cr_{0.6}Al$: an augmented space approach

Monodeep Chakraborty [a]

[a] S.N. Bose National Centre for Basic Sciences, JD-III, Salt Lake City, Kolkata 700098, India

Atisdipankar Chakrabarti [b]

[b] Ramakrishna Mission Vivekananda Centenary College, Rahara, West Bengal, India

Abhijit Mookerjee [c]

[c] S.N. Bose National Centre for Basic Sciences, JD-III, Salt Lake City, Kolkata 700098, India

Abstract

In this communication we present a study of the electronic structure of partially disordered bulk and (100) thin film of quaternary pseudo-Heusler alloy $Co_2Fe_{0.4}Cr_{0.6}Al$ in the $L2_1$ phase using the Augmented Space recursion (ASR) in a scalar-relativistic tight binding linear muffin-tin orbitals (TB-LMTO) basis. We study the orbital resolved magnetic moment contributions of the constituents of the alloy. Our theoretical predictions match well with the available experimental observations for the magnetic moments of Fe and Co but they overestimate that of Cr. For a (100) thin film, layer as well as orbital resolved properties have been studied.

Key words: Partial disorder, augmented space recursion, Heusler alloys
PACS: 61.46+w; 36.40.Cg

Email addresses: monodeep@bose.res.in (Monodeep Chakraborty), adc@bose.res.in (Atisdipankar Chakrabarti), abhijit@bose.res.in (Abhijit Mookerjee).

1 Introduction

Halfmetallic Heusler alloys (also known as halfmetallic ferromagnets, HMF) are those class of materials in which the majority spin band is of metallic character, while the minority spin band is semiconducting, with a band gap at Fermi level (E_F). This remarkable property makes them potential candidates for magnetic field sensors and spintronics devices. A large body of literature have been devoted to experimental and theoretical studies of such systems. The first compound to be identified as HMF by de Groot et.al. [1] was NiMnSb. Since then many different kinds of HMF have been reported, such as zinc-blende structured MnAs, CrAs, CrSb [2]–[3], prevoskite structured $La_{0.7}Sr_{0.3}MnO_3$ [4], rutile structured CrO_2 [5] and Co based Co_2MnSn [6].

We focus our attention on the pseudo-Heusler alloys $Co_2Fe_{0.4}Cr_{0.6}Al$. This is a pseudo HMF because unlike HMF it does not show a true gap at E_F in the minority band. Still this is an important material because of its ferromagnetic character at room temperature and at this particular concentration it shows a high magneto-resistance ratio of up to 30% at a relatively low field of 0.1T [7]–[8]. In addition it shows phase separation [9] and tunnel magneto-resistance [10]–[11] at room temperature for the magnetic tunnel junction which utilizes $Co_2Fe_{0.4}Cr_{0.6}Al$ and Co_2MnAl as an electrode.

There have been several theoretical attempts in understanding the electronic and magnetic behavior of Heusler alloys. Among them is the full-potential screened Korringa-Kohn-Rostocker (KKR) method in conjunction with either coherent potential approximation or super cell construction to account for the random distribution of Cr and Fe atoms. Results using fully relativistic version of the KKR-CPA formalism has been reported in reference [7] for x = 0, 0.4 and 1.0 to study the magnetic nature of the alloy. They have studied the $L2_1$, B2 and A2 phases and their combinations separately. For the $L2_1$ phase and for x = 0.4 their site projected magnetic moment for Co, Cr and Fe were 0.94 $_B$, 1.42 $_B$ and 2.92 $_B$ respectively, whereas their experimental values were 1.11 $_B$, 0.36 $_B$ and 2.64 $_B$ respectively. Reference [12] reported super cell based fully relativistic LMTO calculation of $Co_2Fe_xCr_{1-x}Al$ for x= 0, 0.125, 0.25, 0.375, 0.5,0.625, 0.75 and 1. Their observation was, that the concentration and arrangement of Fe played a decisive role in determining the magnetic properties of the alloy and its constituents. Their theoretically calculated magnetic moments for Fe and Co were quite near to their experimental values, but that for Cr was highly overestimated. The large overestimation of the Cr moment is common to all the theoretical approaches. For all other phases their results also show higher magnetic moment than the experimental observations. Miura et.al. [13] theoretically studied the $Co_2Fe_{0.4}Cr_{0.6}Al$ using KKR-CPA formalism. Their findings indicate that spin polarization of $Co_2Fe_xCr_{1-x}Al$ at E_F, decreases with increasing Fe concentration in both the $L2_1$ and B2 phases and disorder effect plays a significant role on the spin polarization (at E_F) at low Fe concentration. Elmers et.al. [14] used magnetic circular dichroism (MCD) and X-ray absorption spectroscopy (XAS) to study the $Co_2Fe_{0.4}Cr_{0.6}Al$ experimentally. From these data they have also obtained site projected magnetic moments using magneto-optical sum rules and have compared them with band structure calculations. Recently there has been a spurt in experimental activity on thin films of

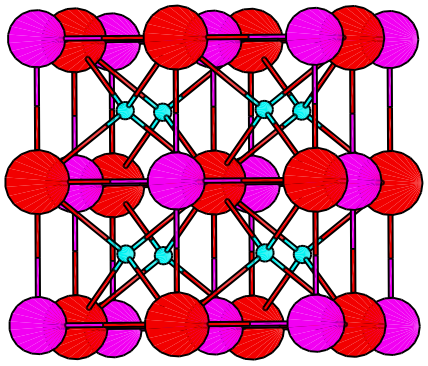

Fig. 1. The unit cell of a Heusler alloy X_2YZ where X and Y are transition metal atoms and Z a sp-metal atom. The medium sized spheres represent Al, large ones are either Fe or Cr and he small spheres represent Co.

Co_2CrAl and Co_2FeAl. Reference [15] reported magnetic properties of both $L2_1$ polycrystalline Co_2CrAl and epitaxial $L2_1$-structured Co_2FeAl films on GaAs(001) substrate. Their observations showed the existence of uniaxial magnetic anisotropy along the [1-10] for Co_2FeAl. On the other hand Co_2CrAl showed an isotropic M-H loop. In an another work Kelekar et.al. [16] reported a method of development of single-phase epitaxial thin films for $Co_2Fe_xCr_{1-x}Al$ and observed large Hall resistivity in the range $(4-5)\times10^{8}$ m at 5 K for x= 0.4.

In this communication we have investigated the magnetic and electronic properties of the bulk and 100 thin film of HMF $Co_2Fe_{0.4}Cr_{0.6}Al$ alloy, using TB-LMTO and ASR formalism. Here we have taken $L2_1$ unit cell with Fm3m symmetry, with experimental lattice parameter a = 5.727 A [7]. The Co site is at 8c$(\frac{1}{4};\frac{1}{4};\frac{1}{4})$ and the Al site is situated at 4a(0;0;0). The Fe and Cr occupy the 4b$(\frac{1}{2};\frac{1}{2};\frac{1}{2})$ site with probability 0.4 and 0.6, respectively. Figure 1 shows the unit cell of a Heusler alloy.

This is an ideal case for for the study of partial disorder (PD) in the $L2_1$ phase. Here the 8c and 4a sites are occupied by the respective atoms with probability 1, and disorder shows up in the 4b sites only. This consideration is of prime importance in order to account for the occupancy of the sub lattice positions in $L2_1$ when we are away from the stoichiometric case (Co_2FeAl or Co_2CrAl). To mimic a free standing Fe/Cr and Al terminated partially disordered thin film of $Co_2Fe_{0.4}Cr_{0.6}Al$, we have considered a nine layer thick films separated by seven layers of empty sphere.

2 Methodology

In this section we generalize the TB-LMTO-ASR formalism to many atoms per unit cell, which is required to study systems having different disorder in different sublattices. Since the recursion method needs a localized, short-ranged basis for its operation, one can implement augmented space recursion in the framework of the TB-LMTO formalism.

The second order TB-LMTO Hamiltonian in the most localized representation is given by,

$$H^{(2)} = E \quad + h \quad h o h \tag{1}$$

where,

$$h = \sum_{RL} (C_{RL} \quad E_{RL}) P_{RL} + \sum_{RL} \sum_{R^0L^{00}} {}_{RL}^{1=2} S_{RL;R^0L^{00}} \; {}_{R^0L^{00}}^{1=2} T_{RL;R^0L^{00}} \tag{2}$$

R denotes a cell position label associated with a TB-LMTO basis and $L = (\ell m m_s)$ is the composite angular momentum index.

is the spin index and denotes an atom in the R-th cell whose position is R + .

C, o and are potential parameters of the TB-LMTO method, these are diagonal matrices in the angular momentum indeces. Also o^{1} has the dimension of energy and is a measure of the energy window around $\tilde{E}$ in which the approximate Hamiltonian $H^{(2)}$ is reliable.

P_{RL} and $T_{RL;R^0L^{00}}$ are the projection and transfer operators in Hilbert space H spanned by tight-binding basis $\{|RL\rangle\}$.

To incorporate disorder in the system, we consider C, o and to be random, while the structure matrix is non random. The justification for the non randomness of the structure matrix is that, we calculate properties of those alloys, where the effect due to individual component size mismatch is negligible. We introduce a site-occupation variable n_R which takes values 0 or 1 depending upon whether site in the R-th cell is occupied by an A or a B atom. In the absence of short-range ordering, the probability density of these variables are given by:

$$Pr(n_R) = x \quad (n_R) + y \quad (n_R \quad 1)$$

x and y are the concentrations of A and B components occupying the labeled atom in the unit cell.

For partial disorder this is a random variable whose probability density depends upon which sublattice it belongs to, hence the label is associated with it. In terms of n_R the random site and angular momentum diagonal potential parameters take the following form:

$$V_{RL} = V_L^A \quad n_R + V_L^B \quad (1 \quad n_R) = V_L^B \; + \; V_L \; n_R$$
$$V_L = V_L^A \qquad V_L^B$$

where, V_{RL} can be any one of C_{RL} , $_{RL}^{1=2}$, o_{RL} and E_{RL} .

We now obtain the Hamiltonian $H^{(2)}$ as a function of the random occupation variables by inserting above expressions in h and nally inserting h in expression (1). To set up the e ective Hamiltonian from which we may obtain the con guration averaged Green function, we follow the prescription of the Augmented space theorem [17]. With each random variable n_R we associate an operator M_R whose spectral density is the probability density of n_R. The theorem tells us that :

$$G \quad (fn_R g;z) \quad = \quad hf;gj \; z\hat{I} \quad \hat{H}^{(2)}(f\hat{M}_R) \quad ^1 \; jf;gi \tag{3}$$

The augmented Hamiltonian $\hat{H}^{(2)}$ is constructed by replacing the random site occupation variables n_R by their corresponding operators $\hat{M}_R$. The eigenstates $j0^R$ i and $j1^R$ i of $\hat{M}_R$ span the con guration space $_Q^R$. The e ective Hamiltonian $\hat{H}^{(2)}$ is an operator in the augmented space $= H \quad ^R$, where H is the space spanned by the TB-LMTO basis jR i. space, A representation of $\hat{M}_R$ is given by

$$M_R = x \; P_R^{"} + y \; P_R^{\#} + \sqrt{x \; y} \; T_R^{"\#} \qquad ^R$$
$$\hat{M}_R = I \quad :::M_R \quad :::I \quad ::: \qquad ^Y \qquad ^R = \tag{4}$$

The representation is in a basis $j"^R$ i = $\sqrt{x}$ $j0^R$ i + $\sqrt{y}$ $j1^R$ i and $j\#^R$ i = $\sqrt{y}$ $j0i$ $\sqrt{x}$ $j1^R$ i. $P_R^{\#}$ = $j\#^R$ $ih\#^R$ j and $T_R^{"\#}$ = $j"^R$ $ih\#^R$ j+ $j\#^R$ $ih"^R$ j are the projection and transfer operators in the con guration space A general con guration state is of the type $j\#""\#$ ::i. The sequence of sites fC g where the con guration is # uniquely describes a con guration. This is called the cardinality sequence. The average con guration is one which has " everywhere : or the null cardinality sequence jf;gi.

A little algebra yields the following : If V_{RL} is a random potential parameter, diagonal in real and angular momentum space (as de ned earlier) then we may de ne the following operators in con guration space :

$$\tilde{A}(V_{RL}) = (x \;\; V_{AL} + y \;\; V_{BL}) \; I \quad :::I \quad :::I:::$$
$$\tilde{B}(V_{RL}) = (y \quad x)(V_{AL} \quad V_{BL}) \; I \quad :::P_R^{\#} \quad :::I \quad :::$$
$$\tilde{F}(V_{RL}) = \sqrt{y \; x} \; (V_{AL} \quad V_{BL}) \; I \quad :::T_R^{"\#} \quad :::I \quad :::$$
and
$$\tilde{D}(V_R) = \tilde{A}(V_R) + \tilde{B}(V_R) + \tilde{F}(V_R)$$

The augmented space Hamiltonian then has the following compact form :

$$\hat{H}^{(1)} = \sum_{RL} \tilde{D}(C_R) \quad P_{RL} \; :::$$
$$+ \sum_{RL} \sum_{R'L'} \tilde{D}(\;^{1=2})_{RL} \; S_{RL;R'L'} \; \tilde{D}(\;^{1=2}_{R'L'}) \quad T_{RL;R'L'}$$
$$\hat{h} = \sum_{RL} \tilde{D}(C_R \quad E_{RL}) \quad P_{RL} \; :::$$
$$+ \sum_{RL} \sum_{R'L'} \tilde{D}(\;^{1=2})_{RL} \; S_{RL;R'L'} \; \tilde{D}(\;^{1=2}_{R'L'}) \quad T_{RL;R'L'}$$
$$\hat{o} = \sum_{RL} \tilde{D}(O_R) \quad P_{RL}$$

Thus :

$$\hat{H}^{(2)} = \hat{H}^{(1)} \quad \hat{h} \; \hat{o} \; \hat{h} \tag{5}$$

Using the augmented space theorem, we can write the expression of configuration averaged Green function as,

$$G_{RL;RL}(z) = \langle 1| z\hat{I} \quad \hat{H}^{(2)} \quad ^{1} |1\rangle$$

where,

$$|1\rangle = |R \quad L \qquad f;g\rangle$$

In order to obtain the Green function we shall use the recursion method of Haydock et.al. [18]. This technique transforms the sparse representation of the TB-LMTO Augmented space Hamiltonian to a tridiagonal form. This is done by constructing a new orthonormal basis set $|n\rangle$ from the older one $|n\rangle$ by the following three term recursion formula :

$$|n+1\rangle = H|n\rangle + \;_n|n\rangle + \;^2_{n\;1}|n \quad 1\rangle \tag{6}$$

with the initial choice $|1\rangle = |1\rangle$, and $\;^2_0 = 1$. The coefficients $\;_n$ and $\;_n$ are obtained by imposing the Otho-normalizability condition of the new basis set. They are given by :

$$\frac{\langle n|H|n\rangle}{\langle n|n\rangle} = \;_n; \quad \frac{\langle n|H|n \quad 1\rangle}{[\langle n|n\rangle\langle n \quad 1|n \quad 1\rangle]^{1=2}} = \;^2_{n\;1}; \quad \langle n|H|m\rangle = 0 \quad (m < n \quad 1) \tag{7}$$

Now the diagonal elements of the Green function can be calculated from the following

expression:

$$G_{RL;RL}(z) = \cfrac{1}{z - \cfrac{\tau_1^2}{z - \cfrac{\tau_2^2}{z - \cfrac{\tau_3^2}{\ddots \; z - \tau_N^2 T(z)}}}} \tag{8}$$

The above infinite continued fraction is terminated after a finite $n = N$ (say) and the asymptotic part is replaced by a terminator calculated from the first N coefficients as suggested by by Beer and Pettifor [19].

The basis site, angular momentum projected density of states (LDOS) is related to the configuration averaged Green function :

$$n_L(E) = \frac{1}{\pi} \lim_{\epsilon \to 0} \mathrm{Im}\, G_{RL;RL}(E - i\epsilon^+) \tag{9}$$

The Fermi energy E_F is obtained from :

$$\int_{-1}^{E_F} dE \sum_L n_L(E) = n$$

where, n is the average valence electrons per cell.

The basis site, angular momentum projected magnetic moment is obtained from :

$$m_L = \int_{-1}^{E_F} dE \; n_L^{\uparrow}(E) - n_L^{\downarrow}(E) \tag{10}$$

3 Results for Bulk $Co_2Fe_{0.4}Cr_{0.6}Al$

First, the electronic structure and magnetic properties of pure compounds is compared with the $L2_1$ partially disordered alloy. The spin resolved total DOS for the three cases $x = 0, 0.4$ and 1 are displayed in figure 2. It shows that the Fermi level is situated in a valley in the minority spin density of states. It is seen that for $x = 0$, spin minority band shows a gap which is a hallmark of HMF, but with increase in the Fe concentration first the gap disappears and then for $x = 1$ it exhibits a sharp dip forming a pseudo gap. This can be understood from the fact, that with the introduction of disorder in the 4b site, the Van Hove singularities are washed away and consequently the band gap in the minority state is filled up. Yet, vestiges of the kink singularities remain in the DOS as a signature of partial disorder. The contribution from majority density of states at E_F

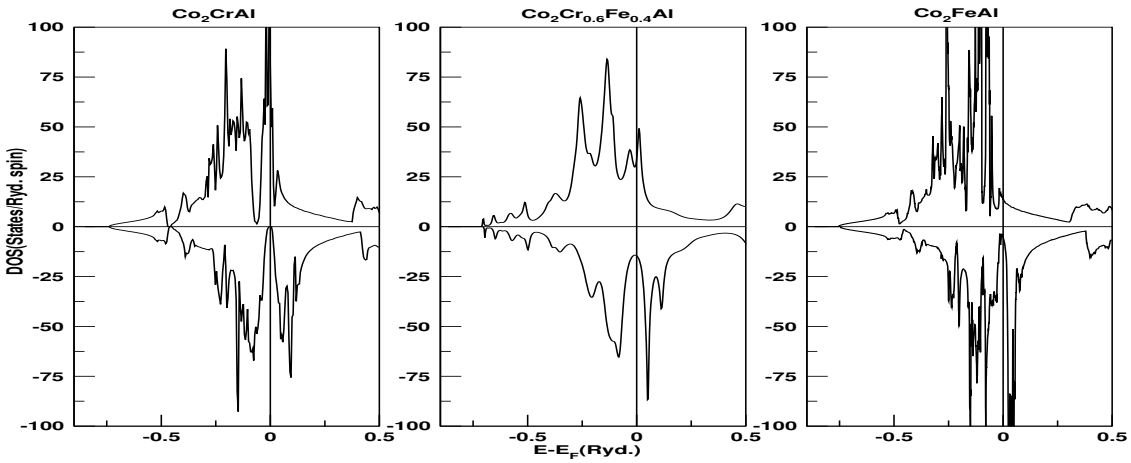

Fig. 2. Total spin resolved DOS of $Co_2Fe_xCr_{1-x}Al$ (x = 0,0.4,1) (center panel) compared with those of Co_2CrAl (left panel) and Co_2FeAl (right panel). Minority states are shown on a negative scale

decreases with increase in Fe concentration. This decrease is monotonic in nature and maximum for Co_2FeAl. A more detail study of the spin resolved site projected DOS (figure 3) reveals that in Co_2CrAl the the bonding states in the minority band is more Co like, where the anti-bonding state is dominated by Cr. The same feature has also been reported by earlier studies. For Co_2FeAl the structures below the Fermi level are dominated by the Co majority band. But above E_F it has contribution from both Co and Fe. In the majority band we see that the two distinct peaks of Fe reinforces the sharp peaks of Co. In the $Co_2Fe_{0.4}Cr_{0.6}Al$ the feature is little different. We see from figure 3 that both Fe and Cr almost retain their structures with respect to parent compounds except the peak in majority band of Cr at the E_F has been shifted slightly towards right. This has major significance in the magnetic moment of Cr which we will discuss later.

The effect of alloying is very prominent in Al and Co. First we observe that the HMF like behavior is lost due to filling up of gap at the E_F in the minority states in these two constituents. Now we discuss the effect of charge transfer on the magnetism of $Co_2Fe_{0.4}Cr_{0.6}Al$ alloy. Table-3 displays the element specific spin resolved charges and total magnetic moment. For Co and Fe our calculated values are closest to the experimental observations although the Cr moment is over-estimated. This over-estimation of the Cr moment has been a recurrent feature of all earlier work. We shall examine whether this is due the accuracy of the electronic structure method used or the way we decide to treat the partial disorder in the system.

From Table-3 we see that the magnetic moment of Cr in the $Co_2Fe_{0.4}Cr_{0.6}Al$ has decreased by an amount 0.576 with respect to Co_2CrAl. This is due the fact that it has lost 0.392 amount of charge (with respect to pure compound) from majority band. A more careful study reveals that major portion of the charge is lost from majority d band. This is also evident in the Cr projected DOS shown in figure 3 where we see that the sharp peak at E_F has been pushed right wards from the Fermi level which accounts for the charge loss. Since the DOS of Fe is almost same with respect to Co_2FeAl, it also retains the value of its magnetic moment. Al shows a small but nonzero magnetic moment and

$Co_2Fe_{0.4}Cr_{0.6}Al$

	Charge									Mag.Mom
	s"	p"	d"	s#	p#	d#	"	#	Tot.	($_B$)
Co	0.346	0.402	4.38	0.345	0.429	3.282	5.127	4.052	9.179	1.075 (1.11*)
Cr	0.294	0.370	2.544	0.299	0.397	1.542	3.209	2.237	5.446	0.972 (0.36*)
Fe	0.348	0.437	4.591	0.345	0.459	1.958	5.38	2.763	8.143	2.617 (2.64*)
Al	0.490	0.692	0.213	0.503	0.764	0.244	1.394	1.511	2.905	-0.117

Co_2CrAl

	Charge									Mag.Mom
	s"	p"	d"	s#	p#	d#	"	#	Tot.	($_B$)
Co	0.332	0.402	4.253	0.320	0.415	3.492	4.987	4.227	9.214	0.760 (0.55*)
Cr	0.284	0.369	3.037	0.284	0.376	1.482	3.69	2.142	5.832	1.548 (0.19*)
Al	0.454	0.675	0.205	0.466	0.718	0.221	1.334	1.405	2.739	-0.071

Co_2FeAl

	Charge									Mag.Mom
	s"	p"	d"	s#	p#	d#	"	#	Tot.	($_B$)
Co	0.306	0.377	4.440	0.312	0.409	3.283	5.123	4.004	9.127	1.119 (1.57*)
Fe	0.333	0.411	4.634	0.326	0.432	1.911	5.378	2.669	8.047	2.709 (2.15*)
Al	0.458	0.646	0.194	0.464	0.713	0.222	1.298	1.399	2.697	-0.101

Table 1
The orbital resolved charges in Fe and Cr atomic spheres in Fe_xCr_{1-x} alloy. Tot. is site projected total charge. * are the corresponding experimental values from Wurhmehl et.al. [7].

it is oppositely polarized with respect to the other constituents in the $Co_2Fe_{0.4}Cr_{0.6}Al$.

We have also studied the variation of the site-projected magnetic moments as a function of the Fe-Cr disorder, which is shown in Figure 4. The trends are very similar to those reported earlier ([7]). The overestimation of the Cr moment, in comparison with experiment, is consistent for all concentrations and of the same order of magnitude as earlier work using di erent theoretical techniques. We shall comment on this in our concluding section.

It would be interesting to compare our density of states results with experimental photoemmission spectra for $Co_2Fe_{0.4}Cr_{0.6}Al$ excited by hard X-rays as reported by Wurmehl [7]. The experimental data (Figure 5) indicate a broad feature of width about 2 eV is seen

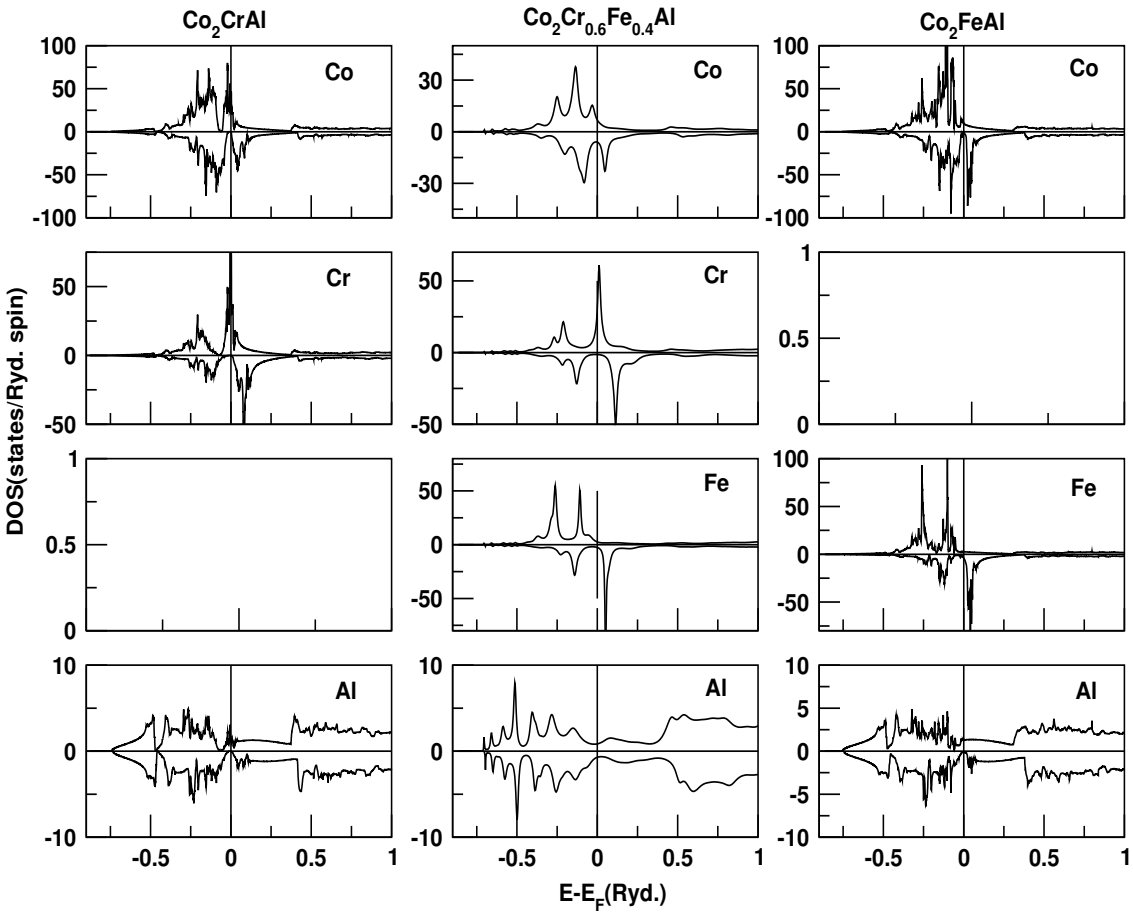

Fig. 3. Site projected spin resolved DOS of $Co_2Fe_xCr_{1-x}Al$ (x = 0,0.4,1). Minority states are shown on a negative scale

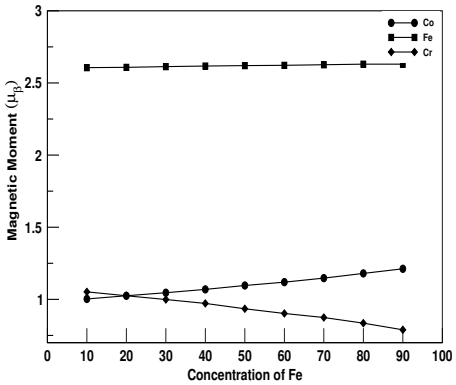

Fig. 4. Variation of site-projected magnetic moments in $Co_2Fe_{0.4}Cr_{0.6}Al$ with the variation in Fe/Cr concentration

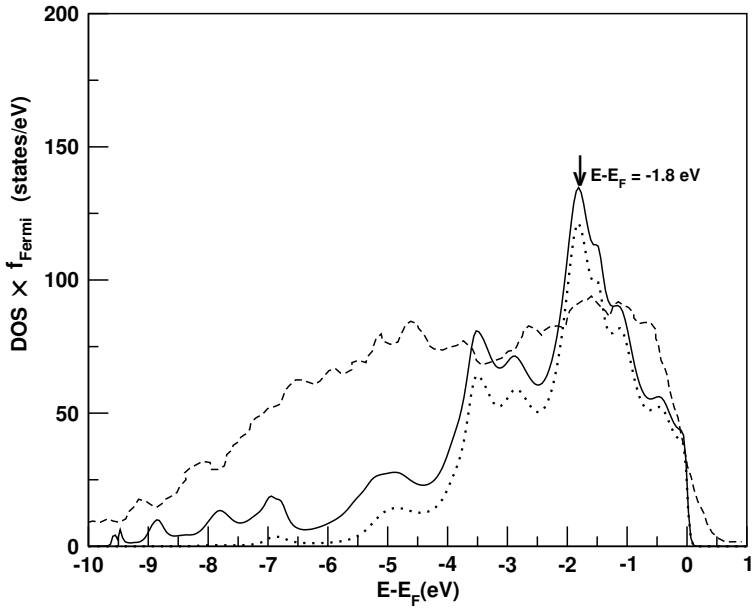

Fig. 5. Comparison between the VB-XPS data of Wurhmehl et.al. ([7]) (dashed lines) and the Fermi function convoluted total density of states (full lines) for $Co_2Fe_{0.4}Cr_{0.6}Al$. The dotted lines show the total d-projected DOS

just below the Fermi energy. A second feature is seen between 4 eV and 7 eV below the Fermi energy. The gure 5 shows the comparison between the VB-XPS data and the total density of states convoluted with the Fermi function corresponding to the experimental temperature. The density of states show two distinct features. First, the structure due to the d-states around and just below the Fermi energy going down almost 5 eV below it. Below this are the features due to the s-p states down to 10 eV below the Fermi energy. The gure shows that the total width of the structures due to the d-states has a width of about 7 eV, which is also the conclusion from the high-resolution, high-energy spectra. The disagreement between the emission spectrum and the total DOS is qualitatively similar to the work of Wurmehl et.al. ([7]). The DOS shows a maximum at around 1.2 eV below the Fermi energy, which is reproduced in the XPS. However, the spectral feature lying from 4 to 7 eV below the Fermi energy is not reproduced at all by the local spin-density approximation based theoretical calculations. This disagreement is qualitatively similar to the earlier works references. Earlier works which ignored disorder suggested that disorder could be a factor, however, our work which includes disorder rules this out. We may speculate, with Wurmehl et.al. [7] that this may point to some de ciencies of the local spin-density approximation.

4 Thin lm and surface of $Co_2Fe_{0.4}Cr_{0.6}Al$

The methodology we have used to study a (100) nine layered thin lm of $Co_2Fe_{0.4}Cr_{0.6}Al$ is same as that of bulk. Here we have carried out a TB-LMTO ASR calculation, to ob-

tain the layer, site as well as orbital (ℓ-m_l-m_s) resolved density of states. The recursion method is ideal for application to systems with surfaces. It was originally suggested by Haydock et.al. ([18]) precisely for such a problem. With these results at our disposal we have performed a detailed analysis of how charge redistributes itself amongst the various orbitals as a result of alloying in the Cr/Fe site and due to the quasi two dimensional nature of the system. The layer resolved DOS are shown in gure 6. All the three Surface states (Al, Fe and Cr) exhibits characteristic surface narrowing due to reduced coordination. The majority surface state of Cr shows a broadening at E_F and is also slightly but importantly shifted towards left, whereas the minority band has almost been pushed out of the E_F, and this is of prime importance, which results in a large increase in the Cr magnetic moment in surface. The majority surface state of Fe does not show much change apart from the fact that the lowest lying peak has broadened out compared to bulk. The structure and height of the minority surface Fe are less developed compared to its bulk counterpart below E_F, whereas above the E_F its structure though prominent, is broadened, left shifted and less sharp than the bulk ones. The layer below the surface layer are occupied by Co and its relative peak width and height have changed with respect to bulk Co. As as we move down to the central layers, they start resembling the bulk DOS for all types. This re ects a very important phenomenon of electronic structure, that the Local density of states is exponentially insensitive to boundary conditions, i.e., the Heine's black body theorem. Table-2 shows the magnetic moments of Cr, Fe and Co in di erent sites (layer projected) of the thin lm and bulk. We can see the magnetic moment for the Cr surface state is spectacularly enhanced whereas for the surface Fe, the enhancement is more conservative. The Co magnetic moment below the surface is slightly suppressed compared to its bulk value. From third layer onwards the magnetic moments are more in tune with their bulk counterparts, which is precisely re ected in the layer variation of the DOS.

Since both Co_2FeAl, Co_2CrAl and $Co_2Fe_{0.4}Cr_{0.6}Al$ have been considered in the $L2_1$ phase, owing to the cubic symmetry of the crystal structure in this phase, the ve-fold degenerate d-orbitals of the atomic case is broken into the three fold degenerate t_{2g} orbitals (d_{xy}, d_{xz} and d_{yz}) and the two fold degenerate e_g orbitals ($d_{x^2-y^2}$ and d_{3z^2-1}). But for a (100) thin lm the z-direction is also rendered inequivalent with respect to x and y directions. This results in further lifting of the degeneracies. Now the out of the ve d-orbitals only two states still retain their degeneracy (d_{xz} and d_{yz}) as a signature of the remnant planar x-y symmetry of the smooth thin lm. In a (100) lm the three orbitals have their lobes (d_{xz}, d_{yz} and d_{3z^2-1}) pointing towards the vacuum and other two ($d_{x^2-y^2}$ and d_{xy}) have their probability distribution perpendicular to vacuum.

Figure 7 shows the spin resolved DOS for constituent d-orbitals of surface Fe (upper panel) and Cr (lower panel) and are compared with their bulk counterparts. Table-3 shows the (ℓ-m_l-m_s) resolved charges and the resulting magnetic moment for surface and bulk states of Fe and Cr.

The Cr majority d_{xy}, d_{xz} and d_{yz} surface states show reduction in peak heights for the lower lying states within E_F whereas the peaks near E_F shows a marked sharpening and are importantly shifted to higher energies. The same can be said about the majority

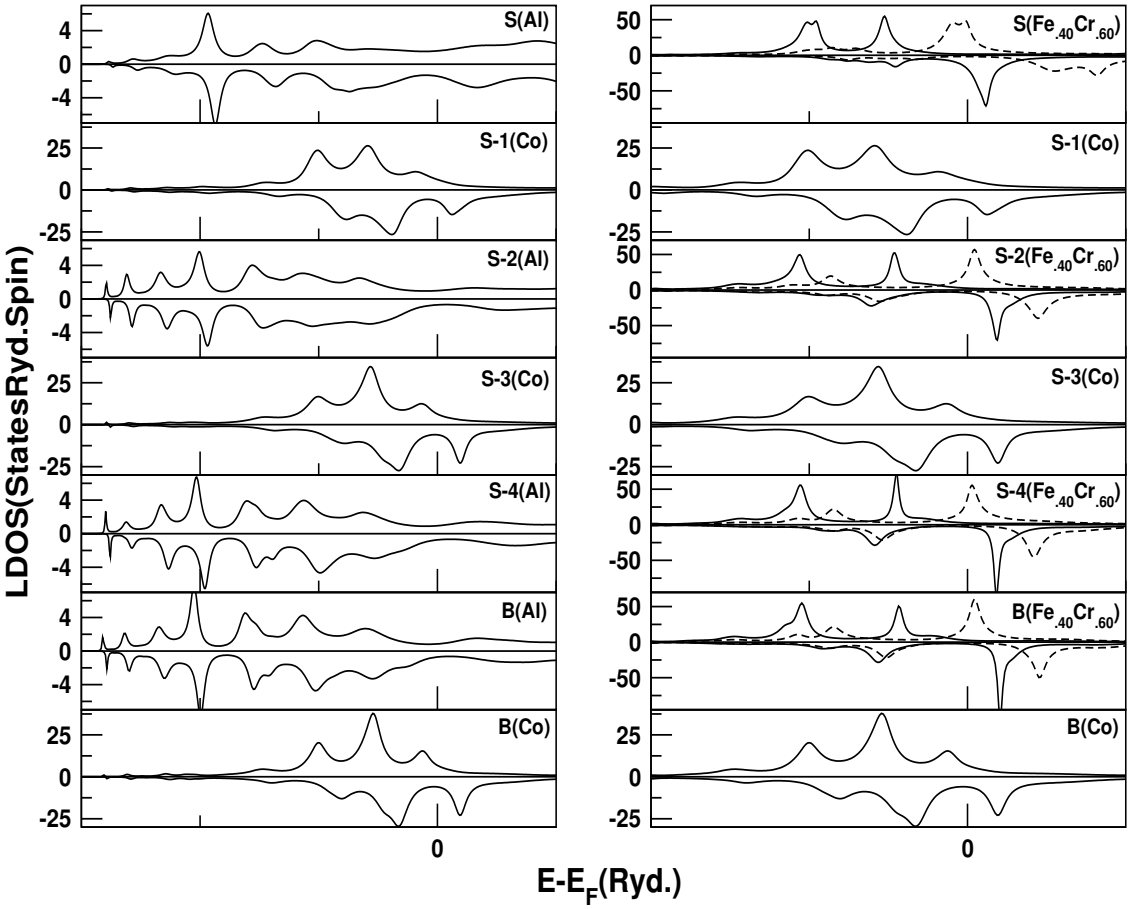

Fig. 6. Site projected spin and layer resolved DOS of $Co_2Fe_{0.4}Cr_{0.6}Al$. Minority states are shown on a negative scale

d_{3z^2-1} state. For the $d_{x^2-y^2}$ state, its peak near E_F is also shifted toward the left, but not sharpened. Below E_F all the minority d-states of surface Cr, with the exception of $d_{x^2-y^2}$, are less sharp than corresponding bulk ones, whereas the structure of the DOS are more developed above E_F. The $d_{x^2-y^2}$ state displays an opposite behavior. Consequently, for Cr each of the majority d-orbitals gain a sizable amount of charge compared to bulk, whereas for minority d-orbitals each of them loses charge, except for a small gain in $d_{x^2-y^2}$ state. This results in a large enhancement in magnetic moment of surface Cr. Since among all the d-orbitals minority state of d_{xy} loses the maximum amount of charge, its enhancement is maximum. The surface enhancement of Cr though remarkable is not surprising, as even for a anti-ferromagnetic thin film of pure Cr, the surface Cr states exhibit a similar enhancement.

Unlike Cr at the surface, where the individual d-orbitals participate in surface enhancement, the magnetic moment of the Fe $d_{x^2-y^2}$ orbital is suppressed. The majority band of the $d_{x^2-y^2}$ state of a surface Fe has its peak near E_F substantially reduced. The main role in the magnetic suppression of surface Fe $d_{x^2-y^2}$ state is played by its minority component. The density of states for minority $d_{x^2-y^2}$ state is pushed below E_F with respect to the corresponding bulk state. This results in a gain in charge in the minority state and

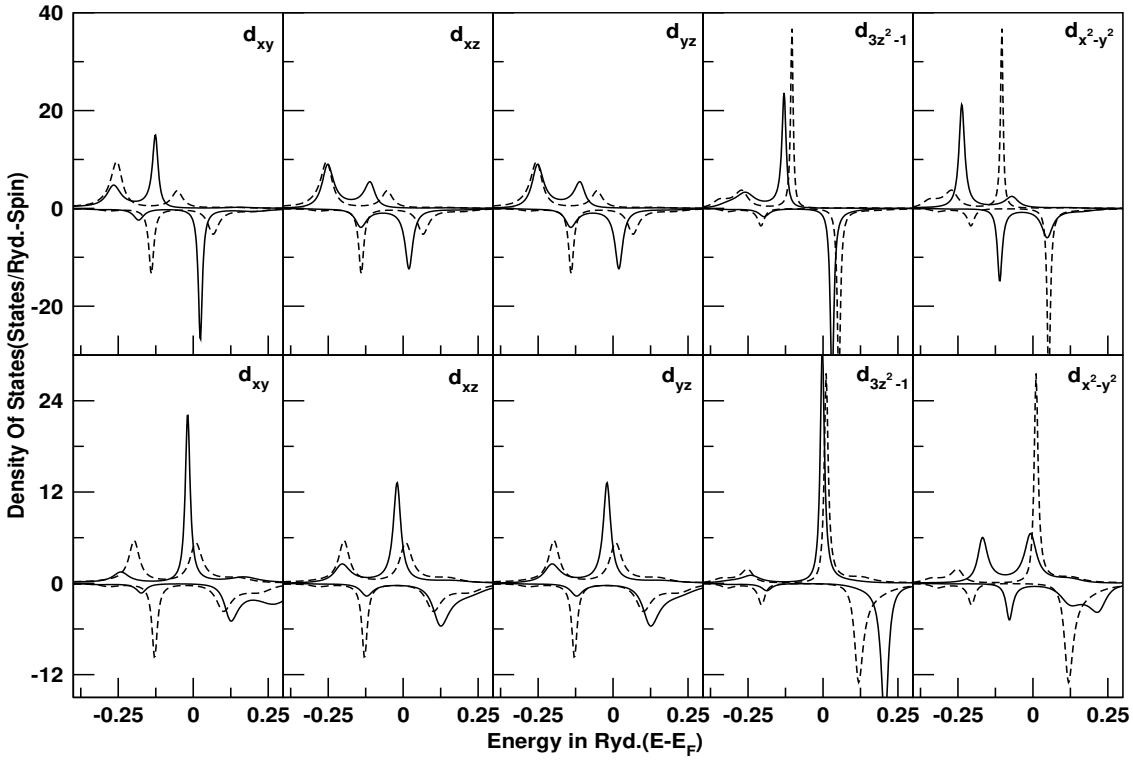

Fig. 7. Spin resolved DOS of different d states of $Co_2Fe_{0.4}Cr_{0.6}Al$. Minority states are shown on a negative scale

	Cr	Fe	Co
S	2.81	2.80	
S-1			0.89
S-2	0.87	2.59	
S-3			1.067
S-4	0.90	2.57	
B	0.97	2.62	1.069

Table 2
The magnetic moment of Fe and Cr and Co for different layers of the thin film and Bulk.

consequent reduction in the moment of Fe.

The Fe d_{xz} and d_{yz} at the surface share a similar fate by virtue of remnant planar symmetry. Their majority sates have their low lying peaks within E_F almost at the same energy as that of the corresponding bulk state, whereas the peaks near E_F, are shifted to its left, resulting in small charge gain. Their minority band at the surface have their peaks near E_F are sharpened as compared to the corresponding bulk state resulting in small loss of charge compared to the bulk. This in turn results in small moment enhancement for d_{xz} and d_{yz}. The surface d_{3z^2-1} of Fe displays similar changes as the d_{xz} and d_{yz} states, when compared to its bulk, with the exception that its peak height near E_F is less than

that of its bulk. As a result its contribution to the surface enhancement is less than d_{xz} and d_{yz} states.

The major contribution to the surface enhancement of Fe comes from the d_{xy} state. The reason for this is that its minority band is almost pushed out of E_F (i.e., to its right). In the majority band the structure near E_F is relatively well developed (i.e., compared to its bulk state) among all the d-states of surface Fe atoms. It is because of the d_{xy} state, that there is an enhancement in moment of surface Fe, despite moment suppression in the $d_{x^2-y^2}$ state at the surface.

5 Summary and Conclusion

We have presented here a version of the TB-LMTO based augmented space recursion technique, modified to include systems with many atoms per unit cell and disorder only in one specific lattice site in the basis. We have shown that the technique is ideally suited to describe the pseudo-Heusler alloy system $Co_2Fe_xCr_{1-x}Al$ both in the bulk and at a surface. We examine the local, component projected magnetic moments, which we believe are sensitively dependent on the accuracy with which we can describe the chemical environment of a component atom. Our predictions agree well with experiment and qualitatively with earlier work. This is with the exception of the gross over-estimation of the Cr moment for all disorder compositions. All earlier work also overestimated the Cr moment quantitatively as much as ours. The question arises, do we understand why this is so?

Miura et al.[13] studied the effect of disorder in the Al and Co sites on the behavior of $Co_2Fe_xCr_{1-x}Al$. They found that disorder between Cr and Al hardly changes matters, while the disorder between Cr and Co leads to a large decrease in the Cr moment. However Antonov et al.[12] argue that such disorder is highly unlikely energetically. That leaves us without a reasonable explanation for the large overestimation of Cr moment. It seems from our work that this discrepancy cannot lie at the door of the type of electronic structure method used (KKR or LMTO) or the method used to deal with the partial disorder (CPA, supercell or ASR).

We speculate that this overestimation may be either due to the use of the Density Functional approximation which cannot take into account correlation in the localized d-states of the constituents properly. Alternatively, one should examine the experimental data in some more detail to determine if sub-lattice disorder does exist because of the way the alloys have been prepared. For the atoms on a (100) surface of $Co_2Fe_xCr_{1-x}Al$ Cr shows a very large enhancement of its local magnetic moment. Fe also shows a moderate enhancement. We have analyzed the atom-spin projected densities of states to try to understand this phenomenon.

Surface

m_l	Charge		Mom.	Charge		Mom.
	Cr"	Cr#	Cr	Fe"	Fe#	Fe
s	0.238	0.225	0.014	0.301	0.285	0.016
p_x	0.082	0.084	-0.002	0.107	0.103	0.004
p_y	0.082	0.084	-0.002	0.107	0.103	0.004
p_z	0.048	0.05	-0.002	0.059	0.057	0.002
d_{xy}	0.720	0.11	0.61	0.94	0.285	0.654
d_{yz}	0.725	0.147	0.578	0.925	0.464	0.461
d_{xz}	0.725	0.147	0.578	0.925	0.464	0.461
$d_{3z^2\ 1}$	0.678	0.084	0.594	0.972	0.185	0.787
$d_{x^2\ y^2}$	0.654	0.211	0.443	0.913	0.508	0.405

Bulk

m_l	Charge		Mom.	Charge		Mom.
	Cr"	Cr#	Cr	Fe"	Fe#	Fe
s	0.294	0.299	-0.005	0.347	0.345	0.002
p_x	0.123	0.132	-0.009	0.145	0.153	-0.008
p_y	0.123	0.132	-0.009	0.145	0.153	-0.008
p_z	0.123	0.132	-0.009	0.145	0.153	-0.008
d_{xy}	0.572	0.392	0.180	0.892	0.500	0.392
d_{yz}	0.572	0.392	0.180	0.892	0.500	0.392
d_{xz}	0.572	0.392	0.180	0.892	0.500	0.392
$d_{3z^2\ 1}$	0.414	0.182	0.232	0.959	0.228	0.731
$d_{x^2\ y^2}$	0.414	0.182	0.232	0.959	0.228	0.731

Table 3
The orbital ('-m_l-m_s) resolved Fe and Cr projected charges and corresponding magnetic moment for surface and bulk states

Acknowledgments

We acknowledge with pleasure, the helpful discussions with Mr. Kartick Tarafdar of S.N. Bose National Centre for Basic Sciences, Kolkata, regarding energy independent ASR. MC would like to acknowledge the Department of Science and Technology, Govt. of India, for

nancial support. A D C would like to thank Ramakrishna Mission Vivekananda Centenary College, Rahara, West Bengal, for encouraging the research project.

References

[1] de Groot R. A., Mueller F. M., van Engen P. G. and Buschow K. H. J (1983) Phys. Rev. Lett. 50 2024

[2] Shirai M., Ogawa T., Kitagawa I. and Suzuki N. (1998) J. Magn. Magn. Mater 177 1383

[3] Shirai M. (2003) J. Appl. Phys. 93 6844

[4] Pickett W. E. and Singh D. J. (1996) Phys. Rev. B 53 1146–1160

[5] Schwarz K. (1986) J. Phys. F: Metal Phys. 16 L211

[6] Plogmann S., Schlatholter T., Braun J., Neumann M., Yarmoshenko Y. M., Yablonskikh M. V., Shreder E. I., Kurmaev E. Z., Wrona A. and Slebarski A. (1999) Phys. Rev. B 60 6428

[7] Wurmehl S, Fecher G. H, Kroth K, Kronast K, Durr H. A, Takeda Y, Saitoh Y, Kobayashi K, Lin H. J, Schonhense G and Felser C, (2006) J. Phys. D: Appl. Phys. 39 803

[8] Felser C., Heitkamp B., Kronast F., Schmitz D., Cramm S., Durr H. A., Elmers H-J., Fecher G. H., Wurmehl S., Block T., Valdaitsev D., Nepijko S. A., Gloskovskii A., Jakob G., Schnhense G. and Eberhardt W. (2003) J. Phys: Condens. Matter 15 7019–27

[9] Kobayashi K., Umetsu R. Y., Kainuma R., Ishida K., Oyamada T., Fujita A., and Fukamichi K. (2004) Appl. Phys. Lett. 85 4684

[10] Inomata K., Okamura S., Goto R. and Yezuka N. (2003) Jpn. J. Appl. Phys., Part 2, 42 L419

[11] Kubota H., Nakata J., Oogane M., Ando Y., Sakuma A. and Miyazaki T. (2004) Jpn. J. Appl. Phys., Part 2 43 L984

[12] Antonov V. N., Durr H. A., Kucherenko Yu., Bekenov L. V. and Yaresko A. N. et.al. (2005) Phys. Rev. B 72 054441

[13] Miura Y., Nagao K. and Shirai M. (2004) Phys. Rev. B 69 144413

[14] Elmers H. J., Fecher G. H., Valdaitsev D., Nepijko S. A., Gloskovskii A., Jakob G., Schonhense G., Wurmehl S., Block T., Felser C., Hsu P.-C., Tsai W.-L., and Cramm S. (2003) Phys. Rev. B 67 104412

[15] Hirohata A., Kurebayashi H., Okamura S., Kikuchi M., Masaki T., Nozaki T., Tezuka N. and Inomata K. (2005) J. Appl. Phys. 97 103714

[16] Kelekar R. and Clemens B. M. et.al. (2004) J. Appl. Phys. 96 540

[17] Mookerjee A. (1973) J. Phys. C: Solid State Phy. 6 L205

[18] Haydock R., Heine V. and Kelly M. J. (1972) J. Phys: Condens. Matter 5 2845

[19] Beer N. and Pettifor D. G. (1982), in The Electronic Structure of Complex Systems, ed. P. Phariseau and W. M. Temmerman, NATO ASI Series B, v.113, p 769

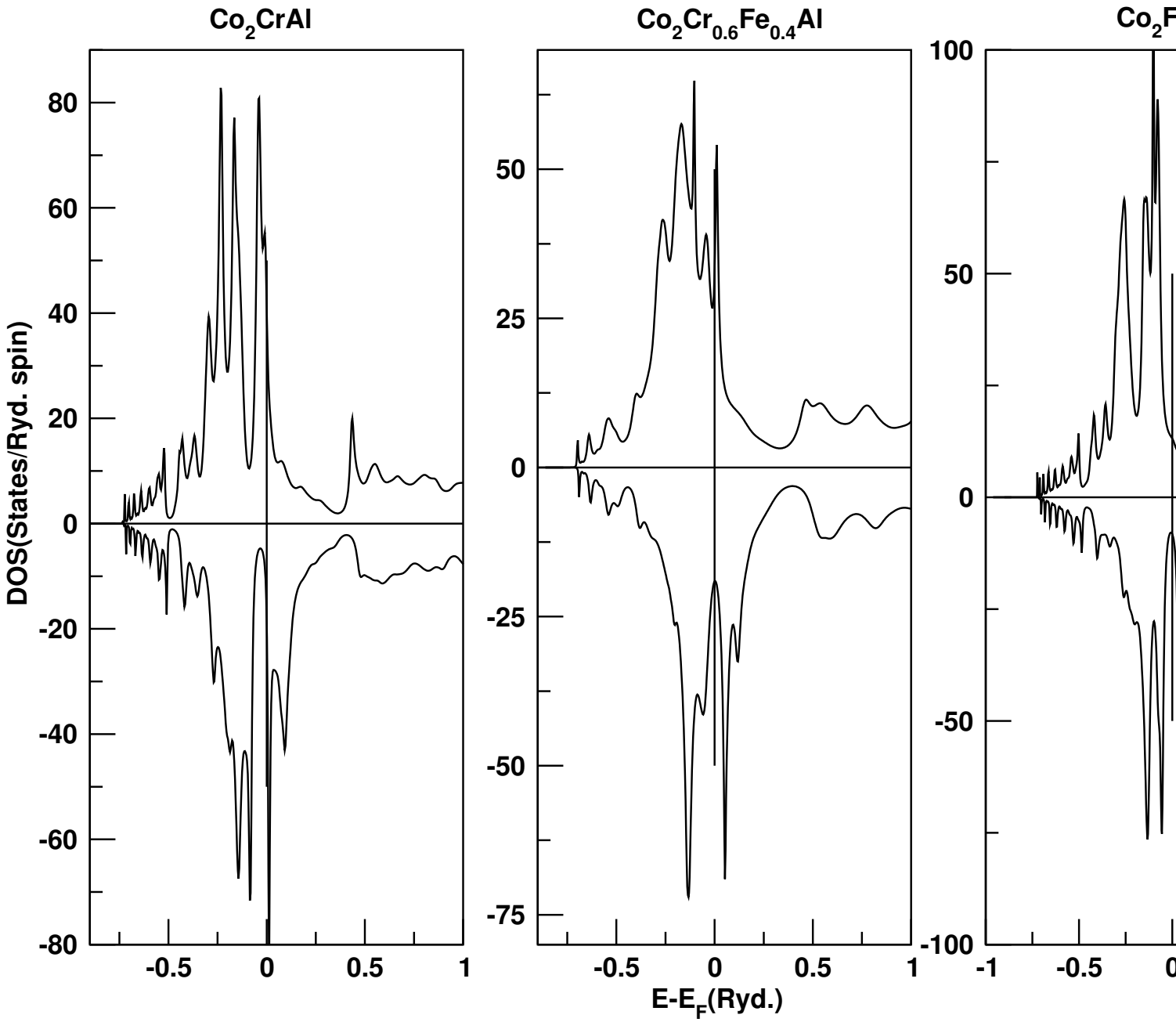
Co2CrAl
Co2Cr0.6Fe0.4Al
Co2F
DOS(States/Ryd. spin)
E-EF(Ryd.)
80
60
40
20
0
-20
-40
-60
-80
50
25
0
-25
-50
-75
100
50
0
-50
-100
-1
-0.5
0
0.5
1